Coupled High-Latitude Climate Feedbacks and Their Impact on Atmospheric Heat Transport

NICOLE FELDL

Department of Earth and Planetary Sciences, University of California, Santa Cruz, Santa Cruz, California

SIMONA BORDONI

Environmental Science and Engineering, California Institute of Technology, Pasadena, California

TIMOTHY M. MERLIS

Department of Atmospheric and Oceanic Sciences, McGill University, Montreal, Quebec, Canada

(Manuscript received 20 April 2016, in final form 22 August 2016)

ABSTRACT

The response of atmospheric heat transport to anthropogenic warming is determined by the anomalous meridional energy gradient. Feedback analysis offers a characterization of that gradient and hence reveals how uncertainty in physical processes may translate into uncertainty in the circulation response. However, individual feedbacks do not act in isolation. Anomalies associated with one feedback may be compensated by another, as is the case for the positive water vapor and negative lapse rate feedbacks in the tropics. Here a set of idealized experiments are performed in an aquaplanet model to evaluate the coupling between the surface albedo feedback and other feedbacks, including the impact on atmospheric heat transport. In the tropics, the dynamical response manifests as changes in the intensity and structure of the overturning Hadley circulation. Only half of the range of Hadley cell weakening exhibited in these experiments is found to be attributable to imposed, systematic variations in the surface albedo feedback. Changes in extratropical clouds that accompany the albedo changes explain the remaining spread. The feedback-driven circulation changes are compensated by eddy energy flux changes, which reduce the overall spread among experiments. These findings have implications for the efficiency with which the climate system, including tropical circulation and the hydrological cycle, adjusts to high-latitude feedbacks over climate states that range from perennial or seasonal ice to ice-free conditions in the Arctic.

1. Introduction

Climate feedbacks have long been recognized as a key piece to understanding Earth's climate sensitivity. Climate sensitivity is the amount of global-mean surface temperature change for a given external forcing, typically defined as a doubling of CO_2. On time scales relevant to anthropogenic warming, feedbacks include atmospheric processes, such as changes in clouds, water vapor, atmospheric lapse rate, and sea ice, which in turn either amplify or damp the climate response to a forcing (Charney et al. 1979; Hansen et al. 1984; Schlesinger 1985). While conventionally defined relative to the globally averaged case, these processes exhibit rich spatial structures and are arguably activated by regional rather than global-mean warming (Armour et al. 2013). An emerging emphasis in the field of climate dynamics is to understand how the spatial pattern of climate feedbacks controls the spatial pattern of climate change.

In addition to amplifying or damping the climate response, climate feedbacks exhibit two additional characteristic behaviors: nonlinearities and remote impacts. First, from a Taylor series perspective, nonlinearities may be understood as higher-order terms in the energy balance (Colman et al. 1997; Roe 2009). For instance, both longwave radiative fluxes (Stefan–Boltzmann law) and atmospheric moisture content (Clausius–Clapeyron relation) are nonlinear functions of temperature.

Corresponding author address: Nicole Feldl, Earth and Planetary Sciences, University of California, Santa Cruz, 1156 High Street, Santa Cruz, CA 95064.
E-mail: nfeldl@ucsc.edu

DOI: 10.1175/JCLI-D-16-0324.1

However, nonlinearities may also enter as interactions among feedbacks, which introduce bias in the first-order linear approximation. Second, remote impacts are a consequence of positive feedbacks amplifying the local energy balance (or negative feedbacks damping it), which the atmosphere then accommodates by diverging and converging energy flux meridionally (Feldl and Roe 2013b; Roe et al. 2015; Zelinka and Hartmann 2012). Hence, it is probable that regional interactions between feedbacks affect remote climate responses in a nonlinear manner.

Perturbations to the energy balance, caused directly and indirectly by enhanced greenhouse gas concentrations, affect the meridional energy flux and may manifest as changes in the strength or position of the tropical Hadley circulation or in large-scale extratropical eddies. In a previous study, we related changes in energy transport by the circulation to meridional gradients in climate feedbacks, radiative forcing, and ocean heat uptake, which provides the basis for a diagnostic decomposition of the response of the tropical mean circulation in CMIP5 simulations (Feldl and Bordoni 2016). For the most part these effects are large and compensating. At the level of individual feedbacks, it becomes difficult to grasp intuitively how any single feedback affects the circulation response given their interactive nature. For example, compensation between lapse rate and water vapor feedbacks is well known (Bony et al. 2006; Cess 1975). Assuming the feedbacks act in isolation, we can quantify the contribution of the temperature feedback as a 5%–10% K^{-1} weakening of the Hadley cell and of the water vapor feedback as a 5%–10% K^{-1} strengthening. But does that level of specificity matter if the net result is no change at all?

Naturally, such results are still useful for understanding uncertainty among climate change projections, and moreover any particular coupled model is not required to cancel so neatly. Herein we present a series of idealized modeling experiments designed to reveal the coupling between regional climate feedbacks at a mechanistic level. This is conceptually similar to a perturbed physics ensemble (e.g., Sanderson et al. 2008). In contrast to studies such as Kang et al. (2009), which forces the high latitudes by applying an ocean heat source and sink, or Graversen and Wang (2009), which suppresses the surface albedo feedback, we modify the "sensitivity" of sea ice to warming. Specifically, we manipulate the strength of the surface albedo feedback in order to 1) identify compensating behavior in other feedbacks and 2) assess the impact of the net high-latitude feedback on the remote climate response.

2. Methods

We employ the Geophysical Fluid Dynamics Laboratory (GFDL) Atmospheric Model, version 2.1 (AM2.1; Delworth et al. 2006), in its aquaplanet configuration with daily mean solar zenith angle. This aquaplanet model, with a resolution of 2° latitude × 2.5° longitude, has been used extensively by, for example, Kang et al. (2009) and Feldl and Roe (2013b), and has appeared in model intercomparison studies (Rose et al. 2014; Voigt et al. 2016). Seasonally varying insolation corresponds to modern-day parameters in the control runs, except for eccentricity, which is set to zero. The model is coupled to a slab ocean of fixed depth (30 m) with no oceanic heat transport. Sea ice formation is enabled by introducing an ocean albedo dependence on surface temperature; the surface albedo is increased where surface temperatures are less than 270 K, with no modifications to surface fluxes. Elsewhere, ocean albedo remains a function of zenith angle (Taylor et al. 1996). Control CO_2 concentration is 330 ppm. The ice albedo α_i is systematically varied (0.3, 0.4, 0.45, and 0.5) in each CO_2 quadrupling experiment to manipulate the strength of the surface albedo feedback. The eight simulations are integrated for 40 yr, with the exception of $\alpha_i = 0.5$, which is run for 45 yr (including 15 yr of spinup), to serve as a run from which the others are branched. Monthly climatologies are computed from 30-yr periods.

Feedbacks are calculated using the radiative kernel technique (Shell et al. 2008; Soden and Held 2006; Soden et al. 2008). Individual feedback parameters are the product of the radiative kernel for the relevant climate variable, $K_i = \partial R/\partial x_i$, and the climate change anomaly Δx_i normalized by the local (i.e., zonal-mean annual mean) surface air temperature response ΔT_s to give units of watt per meter squared per kelvin (W m^{-2} K^{-1}):

$$\lambda_i = \frac{\partial R}{\partial x_i}\frac{\Delta x_i}{\Delta T_s}, \tag{1}$$

where R is the net radiative flux at the top of the atmosphere (TOA). Note that the conventional approach for global feedbacks is to instead normalize by the global-mean surface warming; however, the regional feedbacks offer a number of advantages where spatial patterns of warming are of interest (Armour et al. 2013; Feldl and Roe 2013a). We consider the Planck, lapse rate, surface albedo, water vapor, and cloud feedbacks. The Planck feedback is associated with a vertically uniform warming of the surface and troposphere ($x = T_s$), the lapse rate feedback with tropospheric warming that deviates from the vertically uniform profile ($x = T'$), and the surface albedo feedback with changes in surface albedo ($x = \alpha$). For the water vapor feedback, the specific humidity anomaly [$x = \ln(q)$] is divided by the standard anomaly for a 1-K warming assuming no change in relative humidity, to ensure consistency of units with the kernel. The tropopause is defined from

50 hPa in the tropics to 150 hPa at the poles, varying as a function of $100\exp[-(|\phi| - 30°)/60°]^2$ for $|\phi| > 30°$ latitude. Finally, we compute the cloud feedback from the change in cloud radiative effect ΔCRE with corrections for cloud masking of noncloud feedbacks, following Soden et al. (2008). Radiative kernels for this aquaplanet setup are calculated from the $4 \times CO_2$, $\alpha_i = 0.5$ simulation (see the appendix for details).

The sum of the energy adjustments due to individual feedbacks, along with the radiative forcing of CO_2 R_f characterizes the anomalous atmospheric energy balance:

$$\Delta R = \sum_i \lambda_i \Delta T_s + R_f + \mathcal{O}(\Delta T_s^2). \tag{2}$$

Higher-order terms account for the nonlinearity, which is estimated as a residual. In an aquaplanet without ocean dynamics and for equilibrium climate states, anomalous surface fluxes are negligible. To maintain balance, latitudes of amplified TOA radiative flux anomalously diverge atmospheric heat flux, and those of damped radiative flux converge atmospheric heat flux (hereafter "heat" indicates column-integrated moist static energy). Thus we can write the northward energy flux as the zonal and meridional integral of feedbacks and forcing and further split the total atmospheric flux into contributions due to stationary and transient eddies ΔF_e and the mean meridional circulation ΔF_{HC}:

$$\Delta F_{HC} + \Delta F_e = \int_{-\pi/2}^{\phi} \int_0^{2\pi} \left(\sum_i \lambda_i \Delta T_s' + R_f' \right) a^2 \cos\phi \, d\lambda \, d\phi, \tag{3}$$

where ϕ is latitude, λ is longitude, and a is the radius of Earth. Primes denote deviations from the global mean; a uniform feedback term or forcing does not alter transports.

The energy flux by the mean meridional circulation is calculated from the zonal-mean monthly mean meridional wind and moist static energy, and hence its annual mean includes seasonal variability in the Hadley cell. A characteristic feature of the aquaplanet model is that, without the zonal asymmetries associated with continents, stationary eddies do not form and cannot transport momentum, heat, or moisture. In the absence of stationary eddies, the transient eddy energy flux is calculated as the difference between the total monthly atmospheric energy flux and the annual-mean energy flux by the mean meridional circulation.

The mass flux ψ_{max} and energy flux can further be related via the gross moist stability, $H = F_{HC}/\psi_{max}$ (i.e., the effective energy stratification of the tropics; Neelin and Held 1987; Held 2001; Hill et al. 2015). Combining Eq. (3) with gross moist stability and assuming small perturbations, we arrive at the following expression for the fractional change in mass flux by the Hadley cell:

$$\frac{\Delta\psi_{max}}{\psi_{max}} = \frac{\iint \sum_i (\lambda_i \Delta T_s)' + \iint R_f' - \Delta F_e}{F_{HC}} - \frac{\Delta H}{H}. \tag{4}$$

Integrals are as in Eq. (3). For a lengthier derivation, see Feldl and Bordoni (2016). Changes in Hadley cell strength are thus quantified in terms of contributions from feedbacks, radiative forcing, atmospheric eddies, and gross moist stability. Since we focus on fractional changes, the response at latitudes of zero energy flux by the Hadley circulation (i.e., the cell edges) is ill defined. Instead, this analysis best captures the region of the streamfunction extrema. In the following section, we perform a detailed evaluation of changes in circulation strength for each albedo experiment, following Eq. (4).

3. Results

a. Climate feedbacks and atmospheric heat transport

The four experiments, in which the albedo value is specified but areal extent freely interactive, exhibit a wide range of polar amplification under $4 \times CO_2$ (Figs. 1a,b). High-latitude surface temperature change is 5 K in the low-albedo experiment ($\alpha_i = 0.3$) and up to 24 K in the high-albedo experiment ($\alpha_i = 0.5$). All of the simulations reside in the same ice-free equilibrium climate state at $4 \times CO_2$, and hence differences in surface warming reflect differences in the initial mean state. In particular, the high-albedo experiment starts from the coldest climatology, with year-round sea ice cover to nearly 50° latitude, and must warm substantially to reach the same end point as the low-albedo experiment, which only ever forms seasonal (not perennial) sea ice.

The different climate responses are reflected in the different climate feedbacks among the experiments (Fig. 1c). In the tropics, the sums of the diagnosed feedbacks are more similar, though small differences in positive subtropical feedbacks may have a substantial effect on divergence of atmospheric heat flux. However, striking differences in the feedbacks occur at high latitudes: the net feedback is weakly negative (i.e., stabilizing) in the high-albedo experiment and strongly negative in the low-albedo experiment. Naïvely, one might expect this difference to equal the magnitude of the surface albedo feedback, since it is the surface albedo that was perturbed as the experimental design.

Figure 2 shows the annual-mean, zonal-mean feedback parameters. The surface albedo feedback varies in

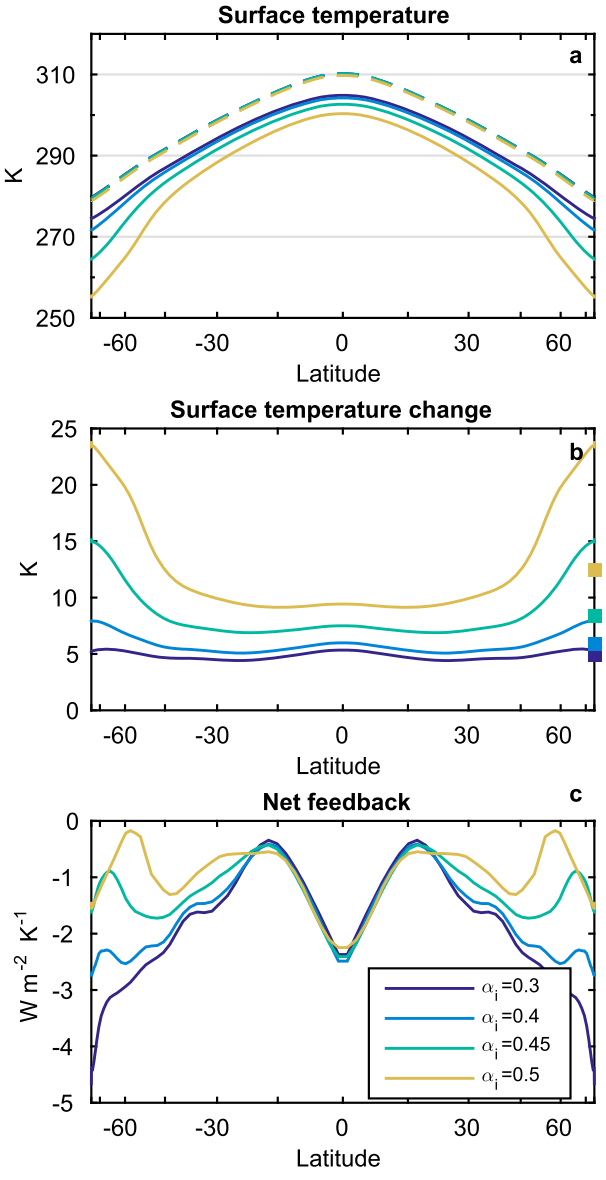

FIG. 1. (a) Annual-mean, zonal-mean near-surface temperature (K) in the 1 × CO_2 (solid lines) and 4 × CO_2 (dashed lines) climates. Note that the instantaneous temperature for sea ice formation is 270 K. (b) Annual-mean, zonal-mean change in near-surface temperature (K) under 4 × CO_2 for the four aquaplanet experiments. Surface albedo values are 0.3 (purple), 0.4 (blue), 0.45 (green), and 0.5 (yellow). Global-mean warming is indicated by the filled squares on the right *y* axis. (c) Zonal-mean net feedback (i.e., sum of linear feedbacks; $W\,m^{-2}\,K^{-1}$).

magnitude and location, with the high-albedo experiment extending the farthest equatorward (a signature of extensive sea ice retreat) and the low-albedo feedback being both weak and of limited areal extent. The feedback magnitude ranges from 0 to 1.4 $W\,m^{-2}\,K^{-1}$, consistent with comprehensive models despite the idealized nature of these simulations (Feldl and Bordoni 2016). Already, we see this difference is not large enough to account for the spread in the net feedback in Fig. 1c. As a consequence of our feedback definition, the Planck feedback is the same in all experiments because $\Delta T_s/\Delta T_s$ is unity, so this is simply the temperature kernel [Eq. (1)]. The lapse rate feedback is positive in the high-albedo experiments and negative in the low-albedo experiments, which we discuss in more detail later in the section. The well-known compensation between water vapor and lapse rate feedbacks (Soden and Held 2006) leads to only small variability in the combined temperature and water vapor feedback. This combined feedback, not including the Planck feedback, is neutral for the low-albedo experiment at high latitudes (not shown).

The cloud feedback is the only remaining feedback capable of contributing to the differences in net feedbacks. Unlike the case for temperature and water vapor feedbacks, the combined effect of surface albedo and cloud feedbacks increases rather than decreases the spread among the net feedback (a positive covariance). This is evident in the high-albedo experiment having the most positive surface albedo *and* net cloud feedback, whereas the low-albedo experiment has the most negative of both feedbacks. At high latitudes, the SW cloud feedback is negative and the LW cloud feedback is positive, resulting from complex interactions among clouds of different thicknesses, heights, and optical properties (Ceppi et al. 2016; Zelinka et al. 2012).

Figure 3 shows the anomalous northward atmospheric energy fluxes implied by the spatial patterns of feedbacks and radiative forcing, as well as the anomalous atmospheric eddy energy flux, following Eq. (3). The fluxes are scaled by global-mean surface temperature change. Positive high-latitude feedbacks produce anomalous energy divergence and an equatorward flux (lapse rate and surface albedo feedback), whereas positive tropical and/or negative high-latitude feedbacks (water vapor and net cloud feedbacks) produce a poleward energy flux. Feldl and Bordoni (2016) show the same result for CMIP5. In contrast to Fig. 2, here the Planck feedback term (in units of $W\,m^{-2}$) does vary among experiments because there is no cancellation by ΔT_s. As anticipated based on the structure of the feedbacks (Fig. 2), the surface albedo feedback and the cloud feedback promote opposing tendencies in atmospheric heat flux; however, they do so in a way that adds to rather than subtracts from the spread among feedbacks. For instance, at 45°N the spreads in the northward fluxes implied by the surface albedo and net cloud feedbacks are comparable, 0.06 $PW\,K^{-1}$ each. Their combined spread is then reduced to 0.08 $PW\,K^{-1}$ by temperature and water vapor feedbacks.

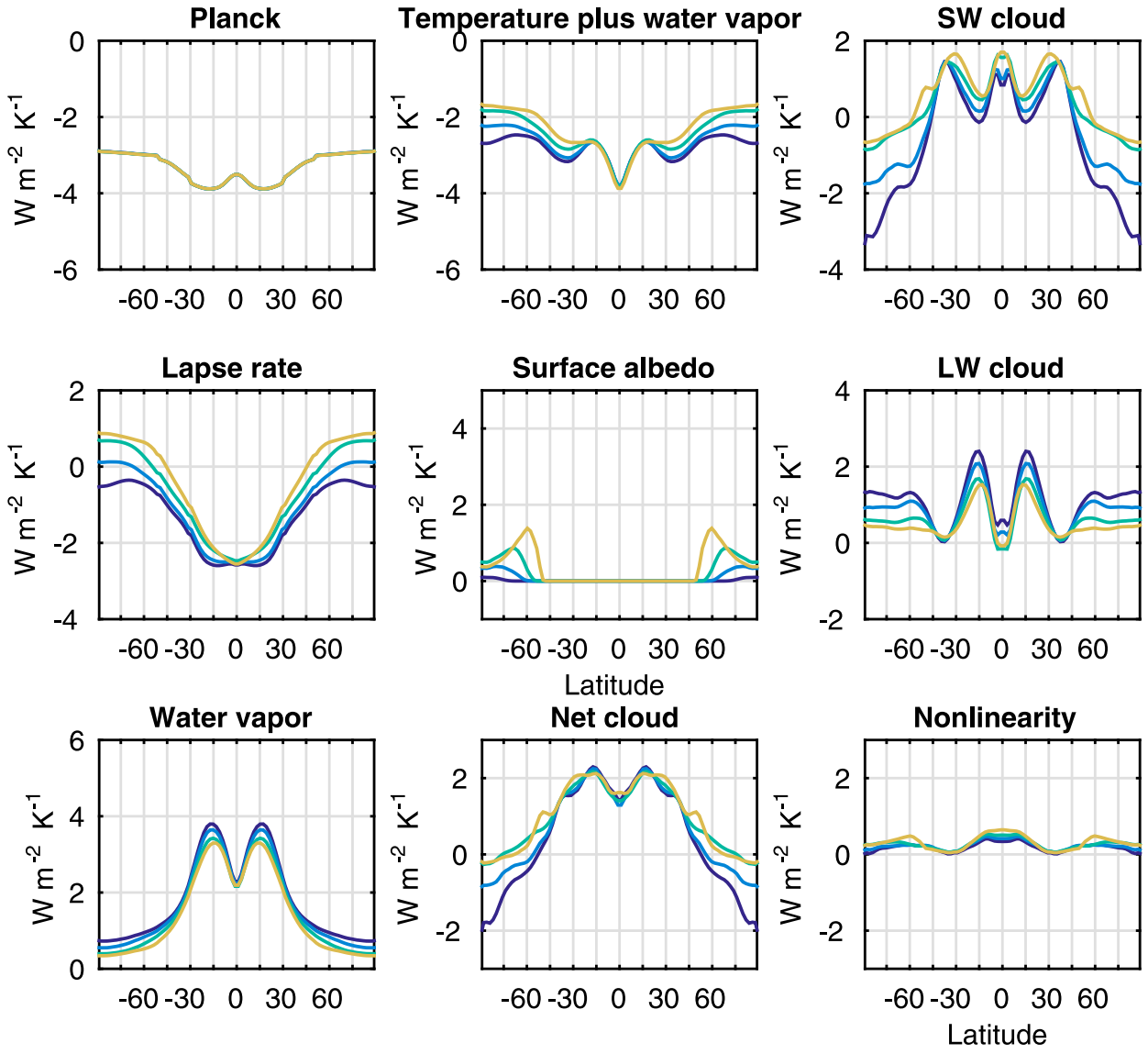

FIG. 2. Annual-mean, zonal-mean regional feedbacks ($W\,m^{-2}\,K^{-1}$) for the four aquaplanet experiments. Simulations are color coded as in the legend of Fig. 1. See Feldl and Bordoni (2016) for the CMIP5 version of this figure.

The bottom panels of Fig. 3 show the role of transient atmospheric eddies (stationary eddies are nonexistent in the zonally symmetric aquaplanet) and radiative forcing. The anomalous flux by eddies is poleward in all experiments in the tropics, but the extratropics show equatorward flux in the high-albedo simulations, consistent with anomalous divergence from the sea ice margin. In not prescribing ocean heat flux divergence, the atmosphere bears the full brunt of transporting heat meridionally. We anticipate the eddy heat flux to be an overestimate compared to coupled atmosphere–ocean models. The notable increase in eddy energy flux in the subtropics is dominated by an increase in latent heat flux, which would occur given the atmospheric moistening on eddy time scales, irrespective of changes in eddy velocities. Finally, our choice of radiative forcing estimate contributes anomalous divergence from the tropics and poleward heat flux, consistent with Huang and Zhang (2014), which we discuss in more detail in section 4.

To evaluate the impact of the coupled climate feedbacks on the strength of the mean meridional atmospheric circulation, it is first helpful to understand the climatological mass and energy fluxes in the aquaplanet simulations. Figure 4a shows the mass flux by the Hadley circulation ψ_{max} in the $1 \times CO_2$ (solid lines) and $4 \times CO_2$

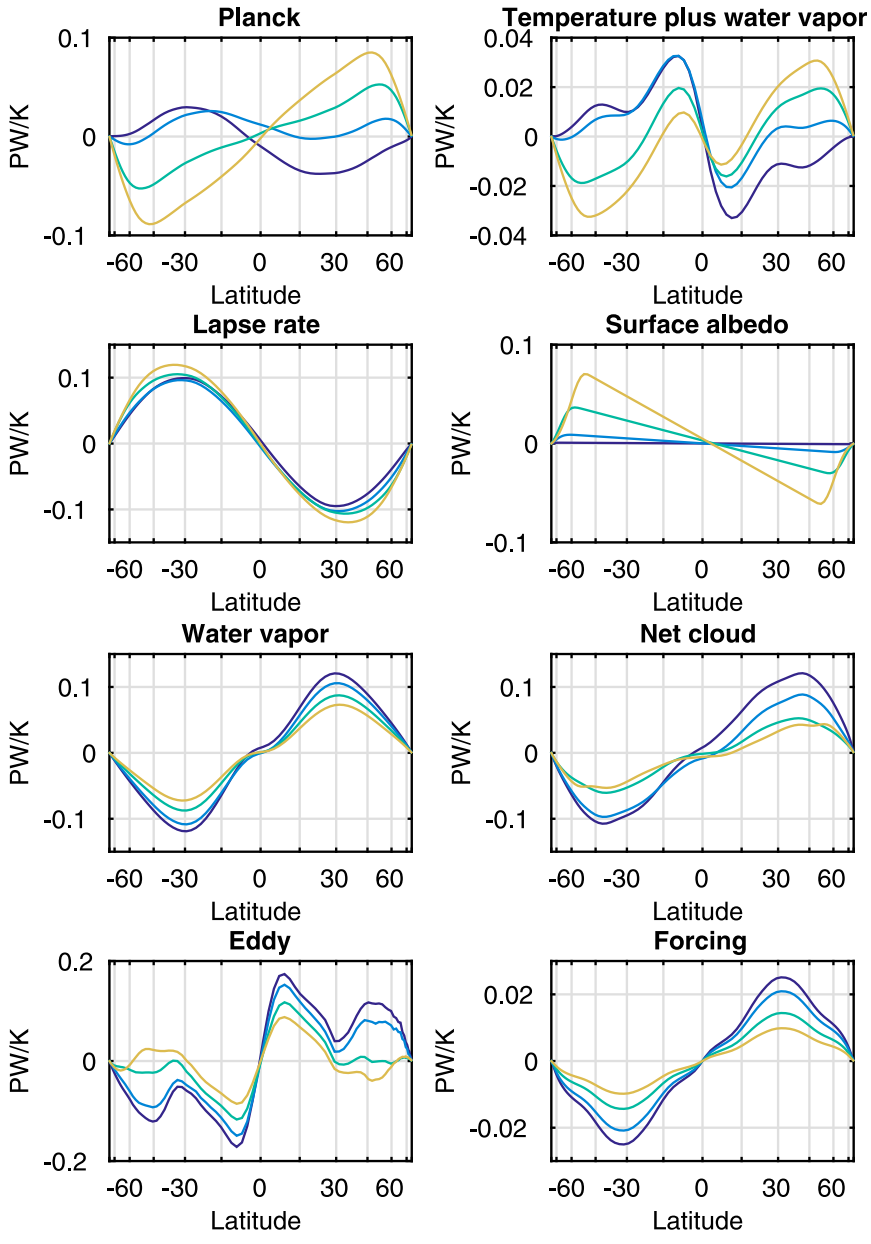

FIG. 3. Anomalous northward atmospheric energy fluxes, integrated from the South to the North Pole. Each experiment is normalized by its global-mean surface temperature change (PW K^{-1}). Simulations are color coded as in the legend of Fig. 1.

(dashed lines) climates. The peak mass flux occurs in the subtropics, and the poleward edges of the Hadley cells are indicated by the latitudes of zero mass flux (near 30° latitude). The high-albedo experiment has the strongest mean tropical circulation and also weakens most. The Hadley cell does expand under increased CO_2, consistent with theory and modeling (Held and Hou 1980; Korty and Schneider 2008; Levine and Schneider 2015; Lu et al. 2007); however, the widening is the same in all four experiments (2° latitude). Hence, the experimental setup induces variability in strength but not position of the Hadley cell. The intertropical convergence zone (ITCZ) remains at the equator in the annual mean, consistent with the hemispherically symmetric model configuration. The northward energy flux by the mean meridional circulation F_{HC} is shown in solid lines in Fig. 4b.

Following Eq. (4), the fractional changes in circulation strength are calculated as the ratio of anomalous fluxes in Fig. 3 to the climatological energy flux in Fig. 4b

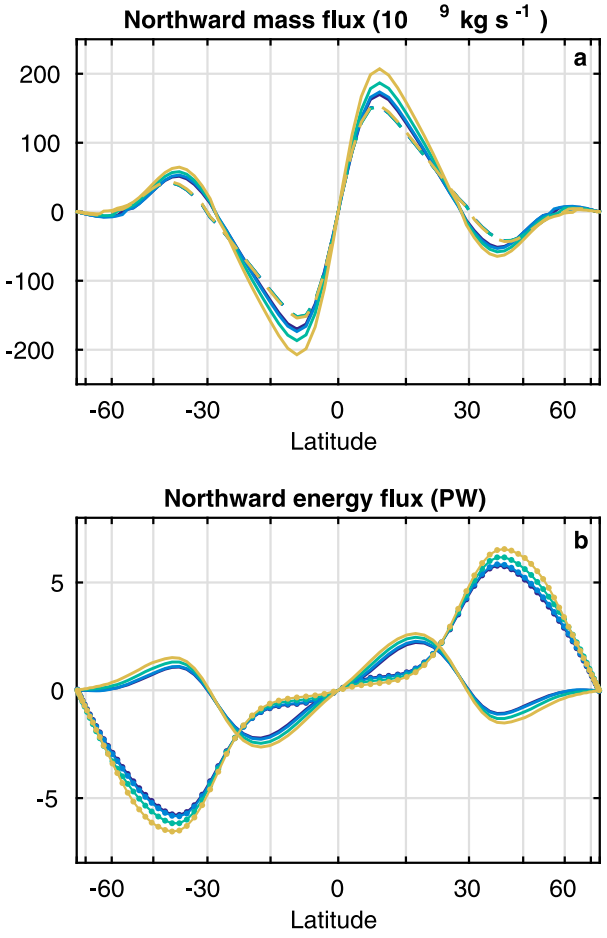

FIG. 4. (a) Annual-mean mass flux in the $1 \times CO_2$ (solid lines) and $4 \times CO_2$ (dashed lines) climates. Mass flux is calculated as the signed maximum magnitude of the meridional mass streamfunction. (b) Annual-mean energy flux by the mean meridional circulation (solid lines) and transient eddies (dotted lines) in the $1 \times CO_2$ climate. Because of the absence of zonal asymmetries, stationary eddies do not occur in the aquaplanet. Simulations are color coded as in the legend of Fig. 1.

(solid lines). Results are averaged over the subtropical latitudes where the Hadley cell, along with its changes, maximizes. Figure 5a shows the circulation changes associated with feedbacks, radiative forcing, gross moist stability, and atmospheric transient eddies. Total decreases (Fig. 5a, leftmost column) range from 1.1% to 1.9% K^{-1}, with the high-albedo experiment exhibiting the largest changes in Hadley cell strength. The greatest contributors to the circulation changes are feedbacks (net strengthening tendency) and eddies (strong weakening tendency). The other contributions are small and positive in most experiments. The increase in tropical energy export by eddies (Fig. 3) is a consistent response to a positive net feedback in the tropics. In previous work, the main compensation occurred instead between atmospheric eddies and ocean heat uptake (Feldl and Bordoni 2016). Here, in the absence of ocean dynamics, that relationship is precluded.

Evaluating the response of the tropical circulation demonstrates the remote impact of coupled climate feedbacks. Given our four experiments are differentiated only by their sea ice albedo formulation, a null hypothesis would have been that the experiments differ only in their surface albedo feedbacks and consequently that the 2.6% K^{-1} spread in circulation change due to the net feedback may be accounted for by the spread in circulation change due to the surface albedo feedback alone. However, in Fig. 5b we see that is not at all the case. The combined temperature and water vapor feedback collapses to a neutral tendency that reduces the spread by 1.3% K^{-1}. The surface albedo feedback is a weakening tendency on the tropical circulation, consistent with the equatorward anomalous energy flux evidenced in Fig. 3. Notably, the spread in the surface albedo feedback contribution is only 1.2% K^{-1} and insufficient to explain the total range of circulation response. The remaining 2.7% K^{-1} is made up by the cloud feedback, a strengthening tendency of 0.8%–3.6% K^{-1}. In other words, the spread—or uncertainty—in surface albedo produces changes in polar clouds that are additive with respect to the uncertainty in the tropical circulation response.

Nonlinear processes account for 4.0 W m^{-2} of the global energy balance in the high-albedo experiment. As a result, the effective climate sensitivity from the sum of the feedbacks underestimates actual global-mean surface warming by about 4 K (8.3 compared to 12.4 K). Largest nonlinearities are found in the $\alpha_i = 0.5$ experiment. Since we use aquaplanet radiative kernels derived from the same reference climate state as the climate change simulations, the nonlinearity does not stem from a kernel-simulation mismatch. Rather, we attribute the high-latitude nonlinear term to interactions between feedbacks, discussed in more detail below, as well as to processes that are nonlinear functions of surface temperature. An additional peak in the tropics is associated with the limitations of the kernel technique and specifically results in an underestimate of the combined temperature and water vapor feedback. The nonlinearity is 1.0 W m^{-2} for $\alpha_i = 0.3$, which in addition to not having an appreciable surface albedo feedback also exhibits the least warming.

b. *Polar clouds and sea ice albedo*

A documented relationship exists between clouds and sea ice, but the mechanisms involved remain ambiguous. In an intermodel comparison, Huybers (2010) reports a

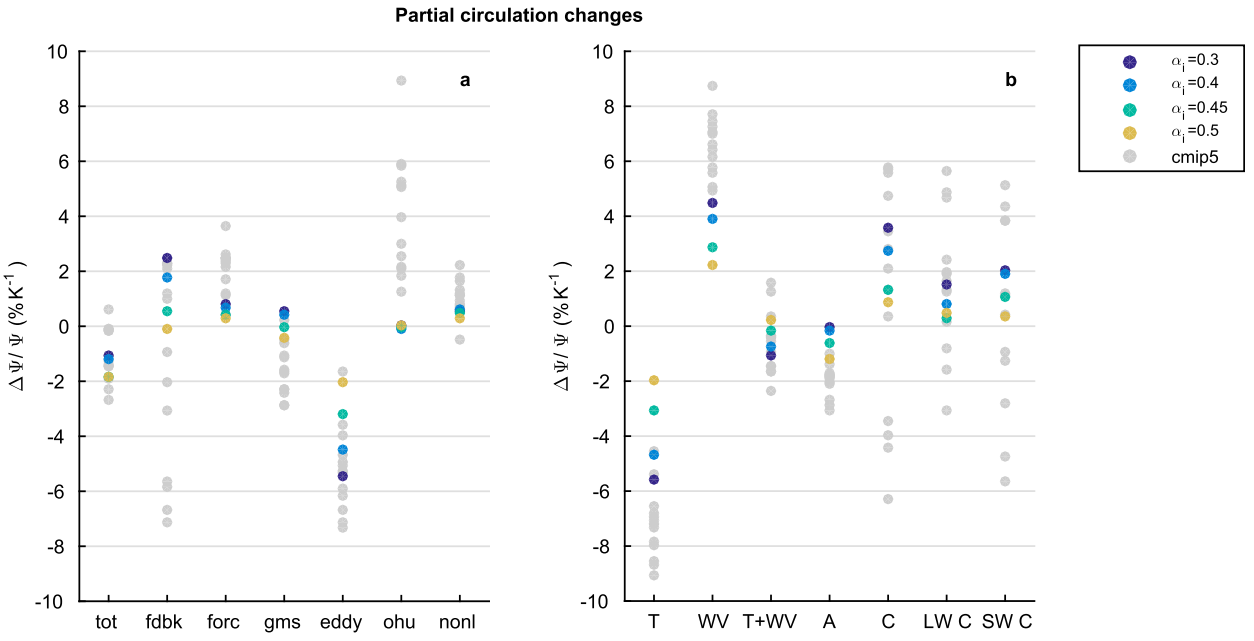

FIG. 5. (a) Changes in circulation strength implied by net feedback (fdbk), radiative forcing (forc), gross moist stability (gms), transient atmospheric eddies (eddy), and ocean heat uptake (ohu) averaged between 15° and 25° latitude in both hemispheres. The total change (tot) is in the leftmost column and the portion of the net feedback due to nonlinearities (nonl) in the rightmost column. The nonlinear contribution is estimated as the residual between the anomalous TOA radiative flux and the sum of feedbacks and forcing, $F_{\mathrm{HC}}^{-1}\int\int\Delta R' - \left(\sum_i \lambda_i \Delta T_s' + R_f'\right)$. Each experiment is normalized by its global-mean surface temperature change (% K^{-1}). CMIP5 results (in gray) are updated from Feldl and Bordoni (2016) to include seasonal variability in the tropical mean circulation and to separate linear from nonlinear feedback contributions. (b) As in (a), but for individual climate feedbacks: temperature (T), water vapor (WV), combined temperature and water vapor (T+WV), surface albedo (A), net cloud (C), and the longwave (LW C) and shortwave (SW C) radiative components of the cloud feedback.

negative covariance between surface albedo and cloud feedback, though the cloud feedback is estimated as a residual and may be biased. Mauritsen et al. (2013) similarly find that cloud and water vapor changes dampen the effect of the surface albedo feedback. One interpretation of these previous studies is that increased cloud fraction masks surface albedo changes, such that the positive surface albedo feedback is weakened relative to clear-sky conditions. One might then anticipate the opposite relationship (i.e., a positive covariance) to develop if the clouds are instead reduced, unmasking surface albedo changes.

Our rationale for focusing our attention on the shortwave radiative component of the cloud feedback is threefold. First, the shortwave cloud feedback dominates the net cloud feedback at high latitudes (Fig. 2). From Fig. 5, we saw that both the shortwave and longwave radiative cloud feedbacks strengthen the tropical circulation and contribute to its spread, but they do so for different reasons: the longwave cloud feedback is a strengthening tendency because it is strongly positive in the subtropics, and the shortwave cloud feedback because it is strongly negative in the extratropics. This latitudinal dependence is related to the seasonal cycle of solar radiation, which produces a maximum in the magnitude of the shortwave cloud feedback in summertime, decreasing to zero for polar night. The longwave cloud feedback in polar regions is a small, compensating effect, insensitive to seasonality.

Second, under a quadrupling of CO_2, we find that polar boundary layer clouds decrease strongly in the high-albedo experiments (Fig. 6). Climatologically in this region, the surface is cold and the atmosphere is stable. Low cloud fraction is large (black lines). By contrast, the low-albedo simulations are relatively warm, lack atmospheric temperature inversions, and have much weaker cloud decks in the initial mean state. The decrease in low clouds, which becomes more pronounced from the low- to high-albedo experiments, is a positive shortwave cloud radiative effect. Enhanced liquid water path in all four experiments ensures an overall negative shortwave cloud feedback, consistent with Ceppi et al. (2016).

The lower-tropospheric stability, estimated as the difference in potential temperature between 700 hPa and the surface, further elucidates the cloud response

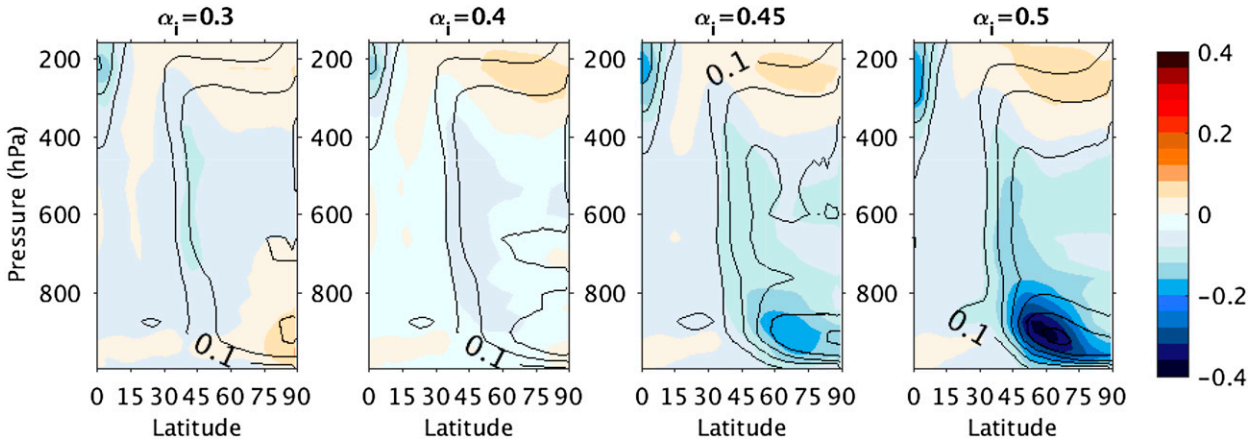

FIG. 6. Annual-mean, zonal-mean change in cloud fraction (shading) and 1 × CO_2 climatology (contour interval is 0.1) for the four aquaplanet experiments.

(Fig. 7). As previously mentioned, the mean 4 × CO_2 climate is identical among simulations (dashed lines). The low-albedo experiments start from a weakly stable atmosphere that increases in stability to reach equilibrium. The high-albedo experiments start from a strongly stable atmosphere that decreases in stability to reach the final state. That decrease in stability is marked by a strong cloud response as the capping inversion at the top of the boundary layer is eroded. The correlation between cloud fraction and lower-tropospheric stability is consistent with common cloud parameterizations (Rasch and Kristjánsson 1998; Slingo 1987). For reference, AM2.1 uses the cloud and convective parameterizations of Tiedtke (1993) and Moorthi and Suarez (1992), respectively.

Third, a physical basis exists for the connection between sea ice and polar clouds. The decrease in planetary albedo associated with the cloud changes is analogous to, and acts in concert with, the decrease in surface albedo due to sea ice retreat. In both cases, the resulting increase in absorbed shortwave radiation warms the boundary layer, contributing to the characteristic bottom-heavy polar warming profile. In both cases, where clouds and sea ice are initially more extensive, potential decreases may also be larger. And in both cases, uncertainty in the magnitude of the response contributes to the total uncertainty in atmospheric heat transport. Critically, while the SW cloud feedback is negative, the mechanisms described above render it ''less negative'' in the high-albedo experiment relative to the low-albedo experiment. Polar cloud and sea ice changes thus amplify the energy imbalance at high latitudes, requiring less poleward heat transport under enhanced CO_2. In the high-albedo experiments, that decrease is accomplished by decreases in energy flux by both transient eddies and the mean meridional circulation. In the low-albedo experiments, the weakening of the Hadley cell alone is sufficient.

4. Summary and discussion

Feedbacks do not act in isolation. When we turn a positive feedback off, the net feedback becomes more negative than can be accounted for based on the strength of the missing feedback alone. In the experiments presented herein, the effect of manipulating the surface albedo feedback is investigated. By restricting the formation of sea ice—in actuality a simple ocean albedo dependence on surface temperature—we simulate the

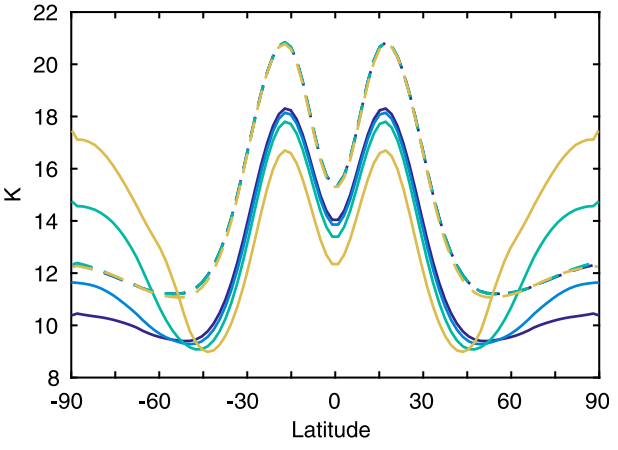

FIG. 7. Annual-mean, zonal-mean lower-tropospheric stability calculated as the difference in potential temperature between 700 hPa and the surface in the 1 × CO_2 (solid lines) and 4 × CO_2 (dashed lines) climates. Simulations are color coded as in the legend of Fig. 1.

transition from perennial or seasonal ice to ice-free conditions. For a warm initial mean state, the characteristic bottom-heavy structure of Arctic warming is inhibited, and boundary layer clouds show slight increases rather than the strong decreases that occur when the lower troposphere is destabilized. Importantly, while the coupled climate feedbacks explored are extratropical in nature, the impacts are global. The net feedback has a stronger meridional gradient in the low-albedo experiment, which reinforces the existing pole-to-equator temperature gradient and promotes an anomalous poleward flux of energy. The high-albedo experiment ($\alpha_i = 0.5$) behaves in the opposite manner. The strong surface albedo feedback provokes an anomalous divergence of heat flux from the sea ice margin, the signature of which is a decrease in energy flux by extratropical eddies as well as by the tropical Hadley cell. In the tropics, particularly in the low-albedo experiment ($\alpha_i = 0.3$), increased energy export by eddies, which would otherwise be accommodated by the Hadley cell, reduces the spread among the experiments while the coupled high-latitude feedbacks increase it. Taken as a whole, the range in tropical circulation responses can thus be understood in terms of the spatial pattern of coupled climate feedbacks.

An important result from the analysis is added insight into the interactive nature of surface albedo and cloud feedbacks. Temperature and water vapor feedbacks are affected as well, though to a lesser degree. In particular, we find that the lapse rate feedback is positive in the high-albedo experiments, contributing to the evident polar amplification as other studies have also shown (Feldl and Roe 2013b; Graversen et al. 2014; Pithan and Mauritsen 2014), and neutral–negative in the low-albedo experiments. The sign change of the lapse rate feedback is consistent with work by Cronin and Jansen (2016), in which the lapse rate feedback was found to be positive in the presence of surface forcing and negative in the presence of warming by atmospheric heat transport. In our case, boundary layer warming is provided by the surface albedo feedback; in the absence of a strong albedo feedback, the polar warming structure is instead dominated by meridional transport. Ongoing research is aimed at uncovering the mechanisms responsible for the varying amounts of polar amplification in the aquaplanet experiments.

Previous work has demonstrated that polar amplification persists (albeit in a reduced form) even in the absence of a surface albedo feedback (Alexeev et al. 2005; Roe et al. 2015). In contrast, here we show that warming in the low-albedo experiment is relatively uniform, with maxima at the equator and poles (Fig. 1b).

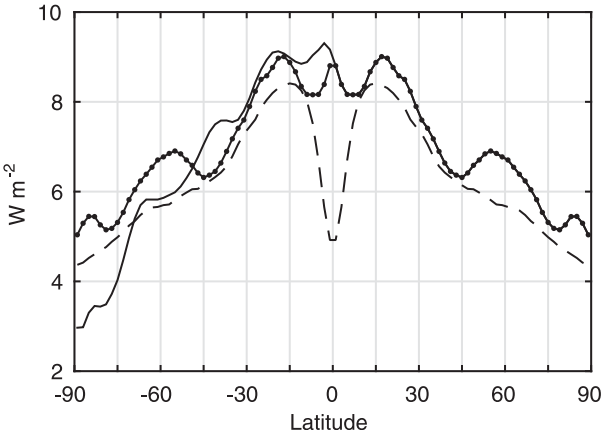

FIG. 8. Annual-mean, zonal-mean radiative forcing for $4 \times CO_2$. Stratosphere-adjusted radiative forcing (dashed line) calculated as $2 \times R_f$ from the GFDL radiative transfer model based on the perpetual equinox aquaplanet simulations of Feldl and Roe (2013b). Fixed-SST radiative forcing (solid line) calculated from the seasonally varying CMIP5 sstClim4xCO_2 and sstClim experiments. Symmetrized fixed-SST radiative forcing used in the present study (dotted line); the global mean is 7.6 W m^{-2}. Note that in the Northern Hemisphere, the two estimates of fixed-SST forcing are identical by design. See Hansen et al. (2005) for more on forcing definitions.

It is tempting to declare the discrepancy a consequence of the inclusion of a seasonal cycle in the present study; however, the feedback structures and mean climates are different enough to render a direct comparison challenging. Regardless, the combination of an extreme feedback gradient and uniform warming pattern in Fig. 1 is evidence of an atmosphere highly effective at redistributing heat between latitudes. If this were not the case, the dominant response would be one of tropical amplification (i.e., greatest warming where feedbacks are most positive).

The inclusion of a seasonal cycle also affects the radiative forcing estimate (Fig. 8). Merlis (2015, 2016) has shown that time-independent and seasonally varying radiative forcing can have different impacts on the annual-mean circulation response. Here we estimate the CO_2 radiative forcing as the ensemble-mean, zonal-mean, symmetrized, and 6-month-lagged forcing from the CMIP5 sstClim4xCO_2 minus sstClim experiments. This fixed-SST forcing includes seasonality, which results in heat flux divergence from the equator. Were a time-invariant forcing instead used, a localized region of convergence due to cloud masking would develop along the equator. Since discussion of tropical circulation within the present study focuses on the regions of streamfunction extrema, this distinction between time-invariant or seasonally varying forcing has little effect. For instance, the partial circulation changes due to radiative forcing are 0.2%–0.5% K^{-1} for the

time-invariant forcing, compared to 0.3%–0.8% K^{-1} for seasonally varying forcing.

We have emphasized the coupling between high-latitude cloud and surface albedo feedbacks. Resulting differences in atmospheric heat transport are felt globally, including by the tropical circulation, which must in turn mediate tropical clouds (Seo et al. 2014; Voigt and Shaw 2015). At the edge of the tropics, the anomalous poleward heat flux implied by the extratropical cloud feedback is 0.1 and 0.04 PW K^{-1} in the low- and high-albedo experiments, respectively (Fig. 3). The edge of the tropics (i.e., 30° latitude) also exhibits differences in low-latitude cloud feedbacks. Since the Hadley cell widens by the same amount in all four albedo experiments, these differences are not due to a differential expansion of the subtropics. Rather, decreases in subsidence are consistent with decreases in tropospheric cloud fraction, and both changes are greatest in the high-albedo experiments.

Interactions among climate feedbacks have been implied based on documented nonlinearities. Here, we demonstrate in a controlled modeling environment how perturbing one feedback, surface albedo, affects the other feedbacks and atmospheric heat transport. Although nonlinear feedback interactions and feedbacks that are nonlinear functions of temperature enter the energy balance at the same order, we may be confident that the former dominates here: 1) The increase in longwave radiative emission with temperature, following the Stefan–Boltzmann law, is a negative nonlinear feedback, and our nonlinearity is positive. 2) The structure of the nonlinearity reveals a peak at approximately 60° latitude in a region of active sea ice and atmospheric processes. We express the degree of coupling between feedbacks in terms of uncertainty in circulation response. For instance, variability in the surface albedo feedback does indeed contribute to the weakening of the Hadley cell; however, the impact is larger than would be expected based on the magnitude of the albedo feedback alone. The implication is that the strength of a feedback cannot be accurately quantified in isolation. Hence, decompositions that emphasize the climate response to individual feedbacks must account for the energy balance residual, which captures the effect of the nonlinear interactions among feedbacks.

Acknowledgments. We thank Dorian Abbot, Tim Cronin, and an anonymous reviewer for their helpful comments on the manuscript. We also thank the editor, Karen Shell. NF was supported by the National Science Foundation (AGS-1524569), and SB was partially supported by the National Science Foundation (AGS-1462544).

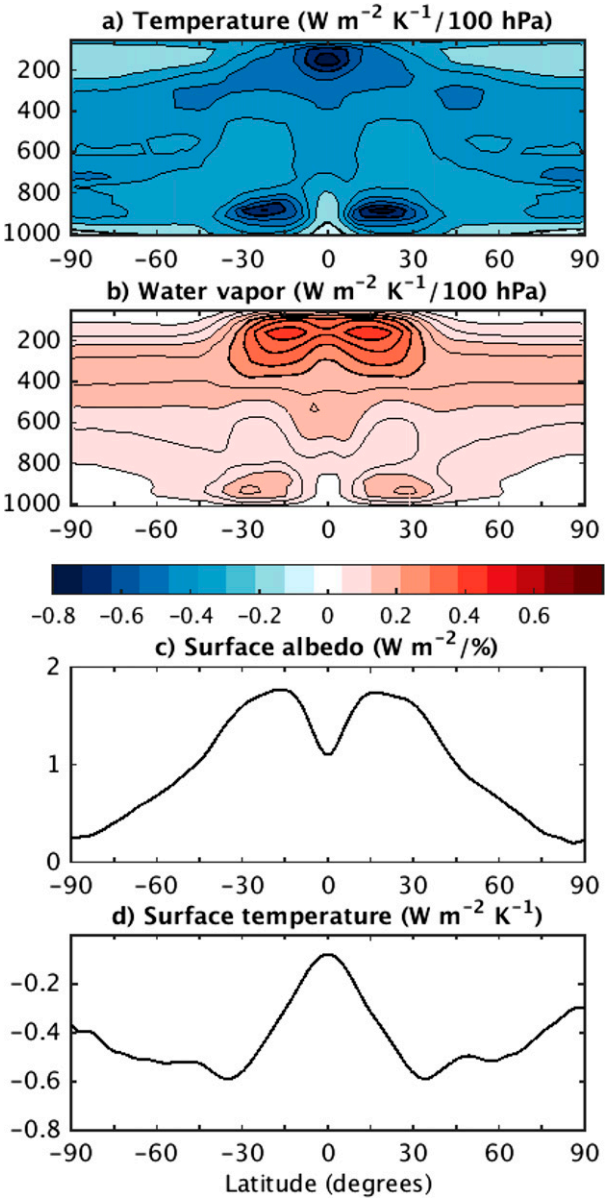

FIG. A1. Annual-mean, zonal-mean radiative kernels for the GFDL AM2.1 aquaplanet based on a 4 × CO_2 simulation with daily mean solar zenith angle: (a) temperature kernel [W m^{-2} K^{-1} (100 hPa)$^{-1}$], (b) water vapor kernel for a specific humidity perturbation corresponding to a 1-K temperature increase and fixed relative humidity, (c) surface albedo kernel, and (d) surface component of the temperature kernel.

APPENDIX

Aquaplanet Radiative Kernels

To compute the aquaplanet radiative kernels, we use a 4 × CO_2 integration of GFDL AM2.1 in the aquaplanet configuration described in section 2. Orbital eccentricity

is set to 0, obliquity to 23.439°, and the solar zenith angle to its daily mean value. While sea ice is permitted via the ocean albedo dependence on surface temperature ($\alpha_i = 0.5$ for SST < 270 K), the mean climate is too warm to form ice, and hence the kernel is effectively ice free. The $4 \times CO_2$ climate is selected over the $1 \times CO_2$ climate because it is identical among our four experiments. This choice of kernel ensures that the feedback estimates are centered on the same reference state for each experiment and that the analysis is unbiased by kernel–simulation mismatch.

Following Soden et al. (2008), a radiative flux calculation is performed eight times daily for a 1-yr simulation. An offline version of the radiative transfer code is then run $2N + 2$ times, where N is the number of vertical levels (24). Temperature is perturbed by 1 K in each layer and specific humidity by an amount corresponding to a 1-K warming, assuming constant relative humidity. Surface temperature and surface albedo are perturbed by 1 K and 1%, respectively. All computations are made for clear skies (clouds instantaneously set to zero) and all-sky conditions. After determining the TOA radiative flux response to each perturbation, we weight the resulting kernels relative to 100-hPa thick layers. Figure A1 shows the zonal-mean, annual-mean temperature, water vapor, and surface albedo kernels for the aquaplanet.

REFERENCES

Alexeev, V. A., P. L. Langen, and J. R. Bates, 2005: Polar amplification of surface warming on an aquaplanet in "ghost forcing" experiments without sea ice feedbacks. *Climate Dyn.*, **24**, 655–666, doi:10.1007/s00382-005-0018-3.

Armour, K. C., C. M. Bitz, and G. H. Roe, 2013: Time-varying climate sensitivity from regional feedbacks. *J. Climate*, **26**, 4518–4534, doi:10.1175/JCLI-D-12-00544.1.

Bony, S., and Coauthors, 2006: How well do we understand and evaluate climate change feedback processes? *J. Climate*, **19**, 3445–3482, doi:10.1175/JCLI3819.1.

Ceppi, P., D. L. Hartmann, and M. J. Webb, 2016: Mechanisms of the negative shortwave cloud feedback in high latitudes. *J. Climate*, **29**, 139–157, doi:10.1175/JCLI-D-15-0327.1.

Cess, R. D., 1975: Global climate change: An investigation of atmospheric feedback mechanisms. *Tellus*, **27A**, 193–198, doi:10.1111/j.2153-3490.1975.tb01672.x.

Charney, J. G., A. Arakawa, D. J. Baker, B. Bolin, and R. E. Dickinson, 1979: Carbon dioxide and climate: A scientific assessment. National Academy of Sciences Tech. Rep., 34 pp., doi:10.17226/12181.

Colman, R. A., S. B. Power, and B. J. McAvaney, 1997: Non-linear climate feedback analysis in an atmospheric general circulation model. *Climate Dyn.*, **13**, 717–731, doi:10.1007/s003820050193.

Cronin, T. W., and M. F. Jansen, 2016: Analytic radiative–advective equilibrium as a model for high-latitude climate. *Geophys. Res. Lett.*, **43**, 449–457, doi:10.1002/2015GL067172.

Delworth, T. L., and Coauthors, 2006: GFDL's CM2 global coupled climate models. Part I: Formulation and simulation characteristics. *J. Climate*, **19**, 643–674, doi:10.1175/JCLI3629.1.

Feldl, N., and G. H. Roe, 2013a: Four perspectives on climate feedbacks. *Geophys. Res. Lett.*, **40**, 4007–4011, doi:10.1002/grl.50711.

——, and ——, 2013b: The nonlinear and nonlocal nature of climate feedbacks. *J. Climate*, **26**, 8289–8304, doi:10.1175/JCLI-D-12-00631.1.

——, and S. Bordoni, 2016: Characterizing the Hadley circulation response through regional climate feedbacks. *J. Climate*, **29**, 613–622, doi:10.1175/JCLI-D-15-0424.1.

Graversen, R. G., and M. Wang, 2009: Polar amplification in a coupled climate model with locked albedo. *Climate Dyn.*, **33**, 629–643, doi:10.1007/s00382-009-0535-6.

——, P. L. Langen, and T. Mauritsen, 2014: Polar amplification in CCSM4: Contributions from the lapse rate and surface albedo feedbacks. *J. Climate*, **27**, 4433–4450, doi:10.1175/JCLI-D-13-00551.1.

Hansen, J., A. Lacis, D. Rind, G. Russell, P. Stone, I. Fung, R. Ruedy, and J. Lerner, 1984: Climate sensitivity: Analysis of feedback mechanisms. *Climate Processes and Climate Sensitivity*, *Geophys. Monogr.*, Vol. 29, Amer. Geophys. Union, 130–163.

——, and Coauthors, 2005: Efficacy of climate forcings. *J. Geophys. Res.*, **110**, D18104, doi:10.1029/2005JD005776.

Held, I. M., 2001: The partitioning of the poleward energy transport between the tropical ocean and atmosphere. *J. Atmos. Sci.*, **58**, 943–948, doi:10.1175/1520-0469(2001)058<0943:TPOTPE>2.0.CO;2.

——, and A. Y. Hou, 1980: Nonlinear axially symmetric circulations in a nearly inviscid atmosphere. *J. Atmos. Sci.*, **37**, 515–533, doi:10.1175/1520-0469(1980)037<0515:NASCIA>2.0.CO;2.

Hill, S. A., Y. Ming, and I. M. Held, 2015: Mechanisms of forced tropical meridional energy flux change. *J. Climate*, **28**, 1725–1742, doi:10.1175/JCLI-D-14-00165.1.

Huang, Y., and M. Zhang, 2014: The implication of radiative forcing and feedback for meridional energy transport. *Geophys. Res. Lett.*, **41**, 1665–1672, doi:10.1002/2013GL059079.

Huybers, P., 2010: Compensation between model feedbacks and curtailment of climate sensitivity. *J. Climate*, **23**, 3009–3018, doi:10.1175/2010JCLI3380.1.

Kang, S. M., D. M. W. Frierson, and I. M. Held, 2009: The tropical response to extratropical thermal forcing in an idealized GCM: The importance of radiative feedbacks and convective parameterization. *J. Atmos. Sci.*, **66**, 2812–2827, doi:10.1175/2009JAS2924.1.

Korty, R. L., and T. Schneider, 2008: Extent of Hadley circulations in dry atmospheres. *Geophys. Res. Lett.*, **35**, L23803, doi:10.1029/2008GL035847.

Levine, X. J., and T. Schneider, 2015: Baroclinic eddies and the extent of the Hadley circulation: An idealized GCM study. *J. Atmos. Sci.*, **72**, 2744–2761, doi:10.1175/JAS-D-14-0152.1.

Lu, J., G. A. Vecchi, and T. Reichler, 2007: Expansion of the Hadley cell under global warming. *Geophys. Res. Lett.*, **34**, L06805, doi:10.1029/2006GL028443.

Mauritsen, T., R. G. Graversen, D. Klocke, P. L. Langen, B. Stevens, and L. Tomassini, 2013: Climate feedback efficiency and synergy. *Climate Dyn.*, **41**, 2539–2554, doi:10.1007/s00382-013-1808-7.

Merlis, T. M., 2015: Direct weakening of tropical circulations from masked CO_2 radiative forcing. *Proc. Natl. Acad. Sci. USA*, **112**, 13 167–13 171, doi:10.1073/pnas.1508268112.

——, 2016: Does humidity's seasonal cycle affect the annual-mean tropical precipitation response to sulfate aerosol forcing? *J. Climate*, **29**, 1451–1460, doi:10.1175/JCLI-D-15-0388.1.

Moorthi, S., and M. J. Suarez, 1992: Relaxed Arakawa–Schubert: A parameterization of moist convection for general circulation models. *Mon. Wea. Rev.*, **120**, 978–1002, doi:10.1175/1520-0493(1992)120<0978:RASAPO>2.0.CO;2.

Neelin, J. D., and I. M. Held, 1987: Modeling tropical convergence based on the moist static energy budget. *Mon. Wea. Rev.*, **115**, 3–12, doi:10.1175/1520-0493(1987)115<0003:MTCBOT>2.0.CO;2.

Pithan, F., and T. Mauritsen, 2014: Arctic amplification dominated by temperature feedbacks in contemporary climate models. *Nat. Geosci.*, **7**, 181–184, doi:10.1038/ngeo2071.

Rasch, P. J., and J. E. Kristjánsson, 1998: A comparison of the CCM3 model climate using diagnosed and predicted condensate parameterizations. *J. Climate*, **11**, 1587–1614, doi:10.1175/1520-0442(1998)011<1587:ACOTCM>2.0.CO;2.

Roe, G. H., 2009: Feedbacks, timescales, and seeing red. *Annu. Rev. Earth Planet. Sci.*, **37**, 93–115, doi:10.1146/annurev.earth.061008.134734.

——, N. Feldl, K. C. Armour, Y.-T. Hwang, and D. M. W. Frierson, 2015: The remote impacts of climate feedbacks on regional climate predictability. *Nat. Geosci.*, **8**, 135–139, doi:10.1038/ngeo2346.

Rose, B. E. J., K. C. Armour, D. S. Battisti, N. Feldl, and D. D. B. Koll, 2014: The dependence of transient climate sensitivity and radiative feedbacks on the spatial pattern of ocean heat uptake. *Geophys. Res. Lett.*, **41**, 1071–1078, doi:10.1002/2013GL058955.

Sanderson, B. M., C. Piani, W. J. Ingram, D. A. Stone, and M. R. Allen, 2008: Towards constraining climate sensitivity by linear analysis of feedback patterns in thousands of perturbed-physics GCM simulations. *Climate Dyn.*, **30**, 175–190, doi:10.1007/s00382-007-0280-7.

Schlesinger, M. E., 1985: Feedback analysis of results from energy balance and radiative–convective models. *The Potential Climatic Effects of Increasing Carbon Dioxide*, M. C. MacCracken and F. M. Luther, Eds., U.S. Department of Energy, 280–319.

Seo, J., S. M. Kang, and D. M. W. Frierson, 2014: Sensitivity of intertropical convergence zone movement to the latitudinal position of thermal forcing. *J. Climate*, **27**, 3035–3042, doi:10.1175/JCLI-D-13-00691.1.

Shell, K. M., J. T. Kiehl, and C. A. Shields, 2008: Using the radiative kernel technique to calculate climate feedbacks in NCAR's Community Atmospheric Model. *J. Climate*, **21**, 2269–2282, doi:10.1175/2007JCLI2044.1.

Slingo, J. M., 1987: The development and verification of a cloud prediction scheme for the ECMWF model. *Quart. J. Roy. Meteor. Soc.*, **113**, 899–927, doi:10.1002/qj.49711347710.

Soden, B. J., and I. M. Held, 2006: An assessment of climate feedbacks in coupled ocean–atmosphere models. *J. Climate*, **19**, 3354–3360, doi:10.1175/JCLI3799.1.

——, ——, R. Colman, K. M. Shell, J. T. Kiehl, and C. A. Shields, 2008: Quantifying climate feedbacks using radiative kernels. *J. Climate*, **21**, 3504–3520, doi:10.1175/2007JCLI2110.1.

Taylor, J. P., J. M. Edwards, M. D. Glew, P. Hignett, and A. Slingo, 1996: Studies with a flexible new radiation code. II: Comparisons with aircraft short-wave observations. *Quart. J. Roy. Meteor. Soc.*, **122**, 839–861, doi:10.1002/qj.49712253204.

Tiedtke, M., 1993: Representation of clouds in large-scale models. *Mon. Wea. Rev.*, **121**, 3040–3061, doi:10.1175/1520-0493(1993)121<3040:ROCILS>2.0.CO;2.

Voigt, A., and T. A. Shaw, 2015: Circulation response to warming shaped by radiative changes of clouds and water vapour. *Nat. Geosci.*, **8**, 102–106, doi:10.1038/ngeo2345.

——, and Coauthors, 2016: The Tropical Rain Belts with an Annual Cycle and Continent Model Intercomparison Project: TRACMIP. *J. Adv. Model. Earth Syst.*, doi:10.1002/2016MS000748, in press.

Zelinka, M. D., and D. L. Hartmann, 2012: Climate feedbacks and their implications for poleward energy flux changes in a warming climate. *J. Climate*, **25**, 608–624, doi:10.1175/JCLI-D-11-00096.1.

——, S. A. Klein, and D. L. Hartmann, 2012: Computing and partitioning cloud feedbacks using cloud property histograms. Part II: Attribution to changes in cloud amount, altitude, and optical depth. *J. Climate*, **25**, 3736–3754, doi:10.1175/JCLI-D-11-00249.1.